

Drug Repurposing Targeting COVID-19 3CL Protease using Molecular Docking and Machine Learning Regression Approach

Imra Aqeel ¹, and Abdul Majid ¹

¹ Biomedical Informatics Research Lab, Department of Computer & Information Sciences, Pakistan Institute of Engineering & Applied Sciences, Nilore, Islamabad 45650, Pakistan; imraaqeel@pieas.edu.pk ; abdulmajiid@pieas.edu.pk

Abstract:

The COVID-19 pandemic has created a global health crisis, driving the need for the rapid identification of potential therapeutics. To meet this challenge, drug repurposing is the only solution with saving cost, time, and labor. In this study, we used the Zinc database to screen the world- approved including FDA-approved 5903 drugs for repurposing as potential COVID-19 treatments targeting the main protease 3CL of SARS-CoV-2. We performed molecular docking and checked the efficacy of drug molecules. To enhance the efficiency of drug repurposing approach, we modeled the binding affinities using several machine learning regression approaches for QSAR modeling such as decision tree, extra trees, MLP, KNN, XGBoost, and gradient boosting. The computational results demonstrated that Decision Tree Regression (DTR) model has improved statistical measures of R^2 and RMSE. These simulated results helped to identify drugs with high binding affinity. From the docking and other statistical analysis, we shortlisted six promising drugs with their respective Zinc IDs (ZINC3873365, ZINC85432544, ZINC203757351, ZINC85536956, ZINC8214470 and ZINC261494640) within the range of -15 kcal/mol to -13 kcal/mol. In the study, the repurposed drugs are novel except ZINC203757351 antiviral compound that has already identified against COVID-19 in other studies. Further, we analyzed the physiochemical and pharmacokinetic properties of these top-ranked selected drugs with respect to their best binding interaction for specific target protease 3CLpro. Our study has provided an efficient framework for drug repurposing against COVID-19. This highlights the potential of combining molecular docking with machine learning regression approaches to accelerate the identification of potential therapeutic candidates.

Keywords: COVID-19; main protease 3CL; drug repurposing; QSAR model; binding affinity; molecular docking

1 Introduction

The COVID-19 pandemic has presented an unprecedented global health crisis, with over 687 million confirmed cases and over 6.8 million deaths worldwide as of May 2023 according to <https://www.worldometers.info/coronavirus/>. Currently, there is no specific drug available to treat COVID-19, and the development of effective therapies has become a priority for researchers globally (Su et al., 2023). COVID-19 is caused by the severe acute respiratory syndrome coronavirus 2 (SARS-CoV-2), a positive-sense single-stranded RNA virus that primarily infects the respiratory tract of humans (Shah et al., 2020). The entry of the virus into host cells occurs when the spike protein binds to the ACE2 receptor on the surface of human cells, and then it utilizes the host's cellular machinery to replicate and spread throughout the body. Fig. 1 depicts the life cycle of coronavirus.

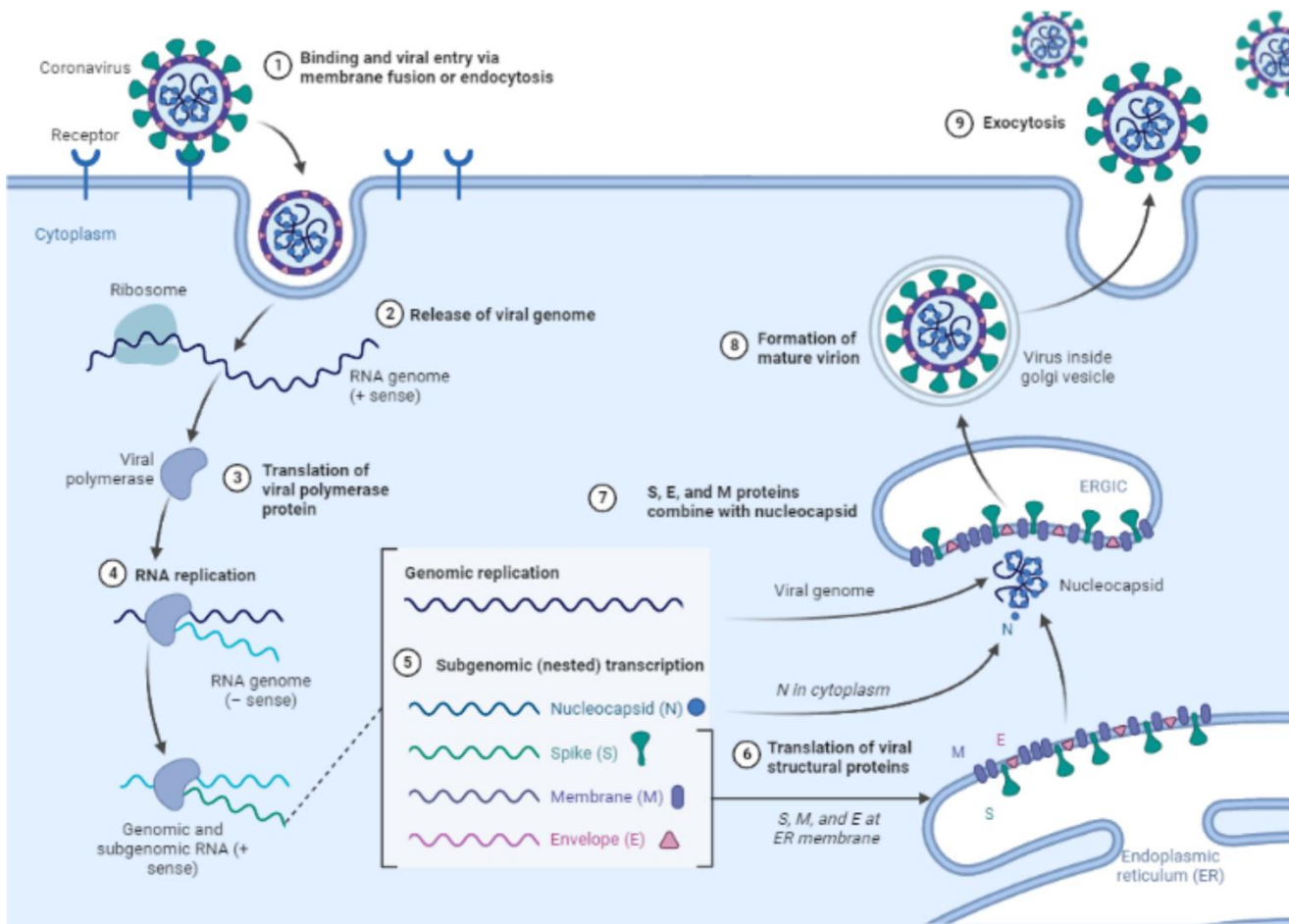


Fig. 1. Life cycle of coronavirus

To support viral replication, SARS-CoV-2 uses various viral proteins, among which the main protease 3CLpro (also called Main protease Mpro) plays a crucial role in cleaving the viral polyproteins into functional non-structural proteins necessary for viral replication. As a result of its significance in the viral life cycle, 3CLpro has become a potential target for the development of antiviral therapies for COVID-19. The catalytic dyad of His41 and Cys145 in the homodimeric cysteine protease 3CL protease makes it an attractive candidate for the development of protease inhibitors (Jin et al., 2020). Several studies have reported the successful identification of small molecules and peptides that can effectively inhibit the activity of the 3CL protease *in vitro*. However, the development of specific and potent inhibitors for the 3CL protease remains a challenge.

In recent years, computational methods have become increasingly important in drug discovery, especially in the early stages of drug development. *In silico* approaches such as molecular docking and machine learning have the potential to accelerate drug discovery by screening large numbers of compounds and predicting their potential binding affinities with target proteins. Molecular docking is a widely used computational method for predicting the binding of small molecules to protein targets. In recent years, machine learning algorithms have been increasingly applied to improve the accuracy of molecular docking predictions. In particular, regression models have been used to predict binding affinities, which are essential for identifying potential drug candidates. In a recent study (Nguyen et al.,

2023), a combination of machine learning (ML), docking, and molecular dynamics (MD) calculations was used and seven representative compounds were identified as having the potential to inhibit SARS-CoV-2 Mpro. In another study (Wang et al., 2023), researchers employed the techniques of molecular docking and molecular dynamic simulation and identified the four drug candidates DB07299, DB01871, DB04653 and DB08732 to combat 3CLpro of SARS-CoV-2.

The repurposing of drugs for COVID-19 involves discovering new therapeutic applications for the existing drugs. It has become a good strategy owing to the pressing need for effective treatments. The approach involves screening existing drugs against SARS-CoV-2 targets, with the aim of identifying compounds that can inhibit viral replication or attenuate the host immune response to the virus. Several studies have used computational methods to identify potential drugs for COVID-19, including 3CL protease inhibitors. For example, in a study (Khan et al., 2023), through the application of molecular docking and simulation techniques, the authors identified two hit compounds, namely CMP4 and CMP2, that exhibit a strong interaction with the 3CL protease. A recent study (Aqeel et al., 2022), we employed a hybrid approach of QSAR, ADMET analysis, and molecular docking to identify potential inhibitors against the 3CL protease of COVID-19. As a result, six bioactive molecules were identified, each with a unique ChEMBL ID: 187460, 222769, 225515, 358279, 363535, and 365134. These compounds demonstrate potential as effective inhibitors of the 3CL protease and could serve as promising candidates for further study and development as treatments for COVID-19. Another study (Elmezayen et al., 2021), utilized virtual screening techniques to repurpose existing drugs for the treatment of COVID-19. The authors identified two drugs, lurasidone and talampicillin, as potential candidates. Additionally, they identified two drug-like molecules from the Zinc database. Molecular dynamics simulation and ADMET analysis were conducted to assess the stability and pharmacokinetic properties of the identified compounds. In a separate study (Jha et al., 2021), molecular descriptors were computed using SVM, logistic regression, and random forest through a deep learning method. This information was then used in QSAR modeling to calculate the binding affinities of protease with drug targets. To develop effective COVID-19 treatments, ML based computational techniques that successfully identify compounds with strong binding affinity have the potential to reduce the cost and time-consuming experiments.

Several recent studies (Ghosh et al., 2023; Infections et al., 2022; Mateen et al., 2023; Adedayo and Famuti, 2023) have reported the effectiveness of repurposed drugs against SARS-CoV-2, such as remdesivir, which has received Emergency Use Authorization by the FDA for COVID-19 treatment, as well as other drugs like diltiazem HCl, mefenamic acid, losartan potassium, mexiletine HCl, glaucine HBr, trimebutine maleate, flurbiprofen, amantadine HCl, dextromethorphan, and lobeline HCl, which have shown promising results in preclinical studies. However, the process of identifying effective repurposed drugs against COVID-19 remains challenging, given the complex and rapidly evolving nature of the disease. Computational approaches, such as molecular docking, have become valuable tools in the identification of potential drug candidates. These methods allow for the rapid screening of large numbers of compounds against specific targets, providing valuable insights into the binding interactions and potential efficacy of the compounds. These studies demonstrate the potential of computational methods in identifying potential drugs for COVID-19, especially those targeting the 3CL protease. However, ML based framework is needed to accelerate the identification of potential therapeutic candidates.

In the study, we proposed ML based framework for drug repurposing in the fight against COVID-19. That framework would help to screen the World-approved including FDA-approved drugs for repurposing as potential COVID-19 treatments targeting 3CLpro. Initially, we retrieved 5903 drug candidates from the Zinc database. We performed molecular docking to evaluate the binding affinities of the drugs towards the target protease 3CLpro using a well-known AutoDock-Vina software (Trott and Olson, 2010). To improve the efficiency of drug repurposing approach, we modeled the binding affinities of the drugs towards the target protease 3CLpro using several ML approaches. Our research highlighted the potential benefit of combining molecular docking with machine learning approaches. The combination of molecular docking and machine learning approaches provides a powerful tool for the rapid screening and identification of potential drug candidates.

In the work, we selected several ML regression models such as Decision Tree regression (DTR), Extra Trees regression (ETR), Gradient Boosting regression (GBR), XGBoost regression (XGBR), Multi-Layer Perceptron regression (MLPR), and K-Nearest Neighbor regression (KNNR). We used the Zinc database to retrieve the world-approved including FDA-approved drugs. We performed molecular docking using a well-known AutoDock-Vina software and evaluated the binding affinities of the drugs towards the target protease. In this next step, 12 diverse types of molecular descriptors were calculated using PaDEL descriptor software (Yap and Wei, 2011). These regression models were trained on these diverse types of feature descriptors. The input dataset was divided into two parts in which 80% data is used for 5-fold cross validation to improve the performance of regression models. The remaining 20% data was used as external data for testing models. The simulated results of Regression model are obtained using statistical measures of R^2 and RMSE. We found that DTR model has improved R^2 and RMSE values as compared to other regression models. Further, DTR model has performed better on ten feature descriptors and outperformed on other two feature descriptors of CDK fingerprint and MACCS fingerprint. This highlights that DTR model is most suitable in predicting the binding affinity. Further, we analyzed the physiochemical properties of these shortlisted compounds with respect to binding interaction to specific target protease 3CLpro.

The subsequent sections of this paper are organized as follows: Section 2 elaborates on the material and the proposed computational framework employed in this study. Section 3 presents the results and corresponding discussions. Finally, Section 4 outlines the concluding remarks of our investigation.

2 Material and Methods

The computational framework proposed in this study is comprised of three modules, as depicted in Fig. 2. Module A encompasses various steps involved in preparing the input dataset. On the other hand, module B illustrates the process of molecular docking, which is used to compute the binding affinities of the drugs with the target protease 3CL. Lastly, module C describes the development of the QSAR model and its performance comparison with different state-of-the-art ML models.

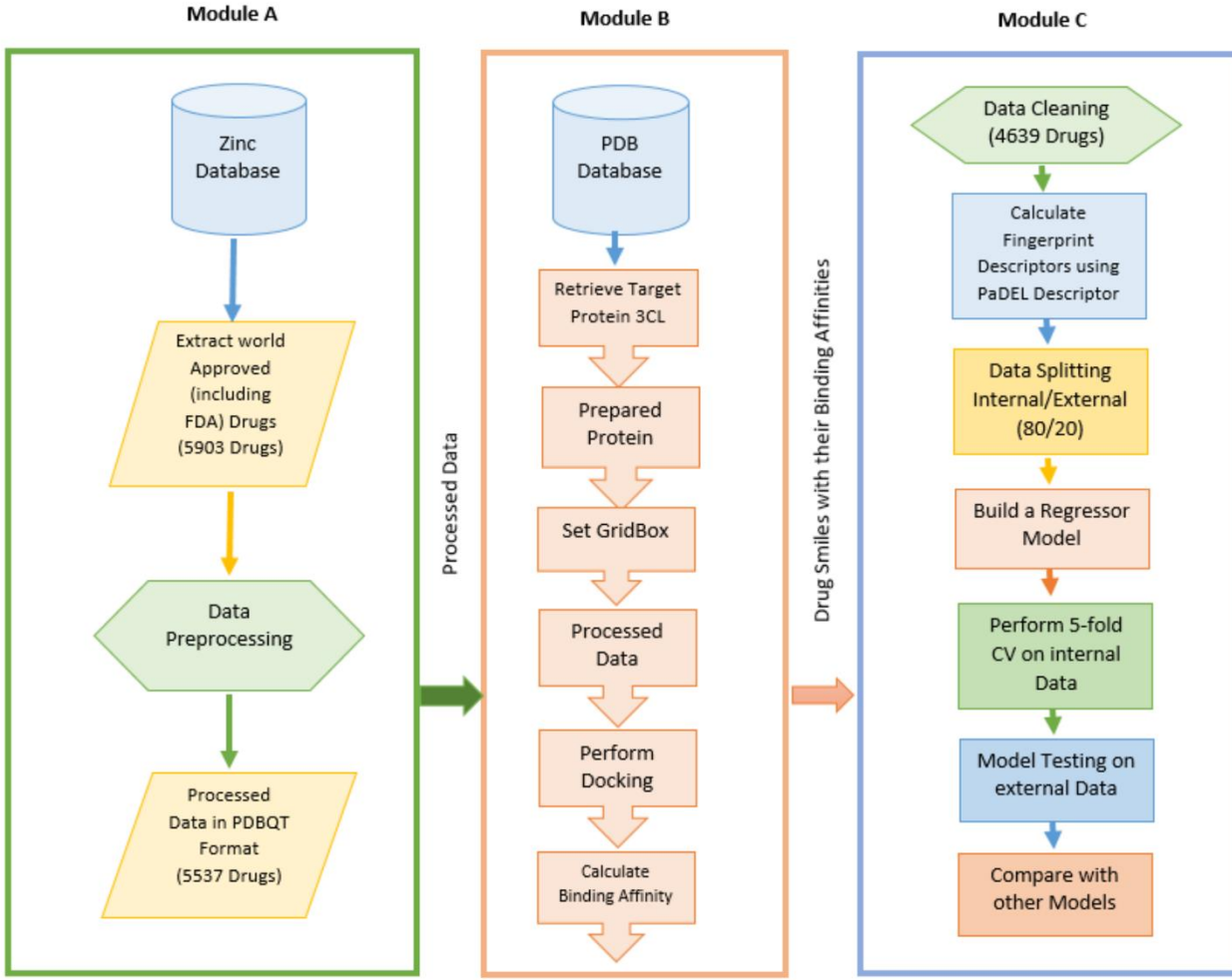


Fig. 2. Three main modules (A to C) in the proposed computational framework

2.1. Module A: Dataset Preparation

Module A outlines various stages of data preprocessing, which are as follows:

2.1.1. Targeting the Viral Enzyme

The 3C-like protease (3CLpro), also known as the Main protease (Mpro), is a critical drug target among the proteins of coronaviruses due to its unique enzymatic properties (Ahmed et al., 2020). This protease, along with the papain-like protease (PLpro), plays a central role in the transcription and replication process of the viral RNA, making it an essential enzyme for the survival and replication of the virus. The high conservation and replication of 3CLpro make it a promising drug target to discover binding inhibitors that can effectively bind to the target protein and potentially inhibit viral replication.

2.1.2. Dataset

The Zinc database is used to retrieve the world-approved including FDA-approved drugs (Irwin et al., 2020). A dataset of 5903 drugs was obtained from <https://zinc20.docking.org/> on (10/02/2023). The Zinc is publically available database having more than 1.4 billion compounds. Every week data is downloaded from this site in terabytes. More than 90% available compounds are verified.

2.1.3. Data Preprocessing

The Zinc dataset consists of 5903 approved drugs that are available in SMILES format. First, these SMILES are converted into SDF format using OpenBabel-2.4.1 software (Boyle et al., 2011). Then, SDF files are converted into PDBQT format so that these drugs can be used to calculate binding affinities towards the target protease. Those files that could not be converted are dropped. After this preprocessing step, the input dataset is reduced to 5537 drugs.

2.2. Module B: Molecular Docking

The 3C-like protease (3CLpro) crystal structure (PDB ID: 7JSU) is retrieved from the RCSB Protein Data Bank on 10/02/2023. Prior to conducting molecular docking, the structure is purified by removing ligands, water molecules, and alternative side chains. The macromolecule is prepared in a charged form by adding polar hydrogen atoms and distributing kollman charges. A GridBox of dimensions 30 x 30 x 30 with a spacing of 01 is fixed to cover the active site of the 7JSU protease, with centers of x, y, and z coordinates are adjusted at -11.046, 12.826, and 67.749, respectively. For molecular docking, Auto-Dock VINA, version 1.2.0 is employed with default parameters (Trott and Olson, 2010). Ligands in PDBQT format are prepared using OpenBabel software. The binding affinities of ligands with target protease are calculated in kcal/mol. The ligand with target interaction with the lowest binding energy is considered the best pose. The crystal structure of the SARS-CoV-2 3CL protease 7JSU, which has a resolution of 1.83 Å, is depicted in Fig. 3.

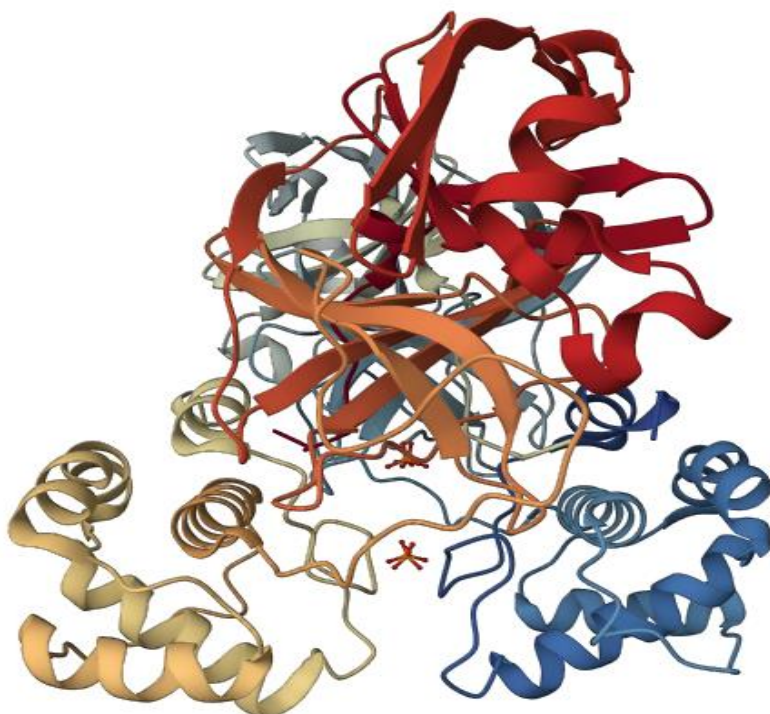


Fig. 3. Crystal structure of SARS 3CL protease 7JSU

2.3. Module C: QSAR Modeling

For QSAR modeling, we have selected several ML based regression models such as DTR, ETR, GBR, MLPR, and KNNR. These models predict the quantitative structure-activity relationship (QSAR) between the biological activities of chemical compounds with unknown properties. These models have successfully established a correlation between the structural characteristics of known chemical compounds with biological activities. The structural properties refer to physicochemical properties that define the compound's structure, while biological activities represent their pharmacokinetic properties. The molecular descriptors of compounds enable the prediction of how changes in structural characteristics affect biological activity (Simeon et al., 2016).

2.3.1. Data Cleaning

To begin the data preparation process for ML models, the dataset undergoes a thorough cleaning procedure to eliminate any instances of data duplication. Additionally, drugs that lack binding affinity values are removed from the dataset to ensure a high quality of data. Following this rigorous cleaning process, the final dataset comprises a total of 4639 drugs that are deemed suitable for subsequent analysis and modeling. The removal of duplicate data and the exclusion of drugs without binding affinity values ensures that the dataset is accurate, reliable, and fit for purpose.

2.3.2. Feature Extraction

The molecular constituents of drug molecules were represented by a vector of fingerprint descriptors. Before computing the descriptors, the PaDEL-Descriptor (Yap and Wei, 2011) software's built-in function was used to standardize tautomer and eliminate salts. In this study, we investigated the effectiveness of 12 diverse fingerprint descriptors to predict the binding affinities of drug molecules. Table 1 provides a summary of the utilized fingerprints, including their respective size, and description,

Table 1: Summary of Twelve Fingerprint Descriptor Sets.

Sr. No	Fingerprint Descriptor	Size (Bits)	Description
1	CDK	1024	CDK fingerprint is a molecular descriptor that encodes structural information of a molecule based on its atomic and bond topology.
2	MACCS	166	The MACCS (Molecular ACCess System) fingerprint is a binary fingerprint representation of a molecule, generated using a predefined set of structural keys.
3	PubChem	881	PubChem fingerprint is a binary fingerprint encoding molecular substructures and functional groups up to a depth of 4 bonds based on PubChem Compound database.
4	E-state	79	E-state fingerprint is a type of molecular descriptor that represents the electronic state of atoms and chemical groups in a molecule.

5	Extended CDK	1024	Extended CDK fingerprint is a fingerprint descriptor that represents molecular structure based on a predefined set of atom-centered fragments, and includes additional features such as atom types, bonds, and ring sizes.
6	2D Atom Pair	780	The Atom Pair fingerprint is a type of molecular fingerprint that encodes the presence of pairs of atoms and their topological distance in a molecule.
7	2D Atom Pair Count	780	2D atom pairs count fingerprint is a type of molecular fingerprint that encodes the frequency of occurrence of atom pairs in a molecule's 2D graph representation. It counts the number of times each atom pair appears in the molecule, and creates a vector of counts for each unique atom pair. The resulting vector represents the 2D atom pairs count fingerprint of the molecule.
8	Graph Only	1024	The Graph Only fingerprint encodes the molecular graph topology, representing the presence or absence of all sub graphs up to a certain size.
9	Substructure	307	A substructure fingerprint is a binary fingerprint representation that encodes the presence or absence of a predefined set of chemical substructures in a molecule.
10	Substructure count	307	Substructure count fingerprint is a type of molecular fingerprinting method that counts the occurrence of predefined substructures within a molecule to generate a binary vector.
11	Klekota Roth	4860	Klekota Roth Fingerprint is a molecular descriptor that encodes the presence and absence of chemical substructures in a molecule.
12	Klekota Roth count	4860	Klekota Roth count fingerprint is a type of molecular fingerprinting method that counts the occurrences of pairs of specific chemical substructures in a molecule.

2.3.3. Decision Tree Regression (DTR) Model

The objective of this research is to develop regression models capable of accurately predicting the continuous response variable, specifically Binding Affinity, by utilizing a range of predictor variables, such as fingerprint descriptors. For this purpose, multiple machine learning (ML) algorithms are developed for quantitative structure-activity relationship (QSAR) modeling. Among these models, the DTR approach is selected due to its superior prediction performance. In machine learning, a DTR (Suay-garcia et al., 2020), (Podgorelec et al., 2002) is a predictive model that uses a decision tree to make predictions. The decision tree is a type of graphical model, consisting of nodes, branches, and leaves,

that resembles a flowchart. Each internal node in the decision tree represents a test on an attribute, each branch represents the outcome of the test, and each leaf node represents a prediction or class label. In a DTR, the value at a leaf node is a continuous value, such as the average or the median of the target values in the training samples that belong to the same leaf node. The decision tree regression model works by recursively partitioning the feature space into subsets, based on the values of the features, in a way that maximizes the reduction of the variance of the target variable. This recursive partitioning process continues until a stopping criterion is reached, such as a maximum depth of the tree or a minimum number of samples required to split an internal node. It has several advantages (Rokach, 2016), such as its interpretability, its ability to handle non-linear relationships between the features and the target variable, and its resistance to over fitting.

The total number of drug molecules in the input dataset, as described in Section 3.3.1, is 4639. This dataset is divided into internal and external datasets with 80 to 20 ratio. The internal dataset is used to train and robust the model performance by employing 5-fold cross validation. For this purpose, 12 diverse type of molecular descriptors, describes in section 3.3.2, are used as the feature sets. The external dataset is used to test the performance of the model.

To evaluate the effectiveness of the developed regression models, two statistical variables, namely R^2 and root mean square error (RMSE), are utilized. The R^2 value is a measure of the proportion of variance in the dependent variable that can be explained by the independent variables. A value of 0 indicates a poor fit, while a value of 1 indicates a perfect fit. On the other hand, RMSE provides a measure of the relative error of the predictive model. To compare the performance of different regression models, a comparative analysis is conducted. For Comparative analysis, we utilized two types of fingerprints as the feature sets. One is CDK Fingerprint and the other one is MACCS fingerprint.

3 Results and Discussion

In this work, we developed several ML based QSAR models for drug repurposing against COVID-19 and predict their binding affinities for approved drugs towards the target protease 3CLpro. First, we will evaluate the performance of our proposed model DTR in predicting binding affinities using twelve distinct features. Then compare its performance with several QSAR models using important statistical measures of R^2 and RMSE. This will help to understand the strengths and weaknesses of each model. Then we will explain the results of molecular docking conducted on the world-approved drugs and their interactions with the target protease 3CLpro. Finally, we will conduct the physiochemical analysis of shortlisted drug compounds with respect to the efficacy of the drugs towards the target protease 3CLpro.

3.1. Evaluation of QSAR Model

The current research proposes a methodology to construct a QSAR model based on the Decision Tree Regression (DTR) algorithm. The model is developed using a dataset of 4639 drug molecules, which is explained in detail in section 2.3.1. To evaluate the performance of the proposed model, 12 distinct types of feature sets are used, as discussed in section 2.3.2. To construct the data matrices, fingerprint features are placed in the X matrix, while Y matrix consists of their corresponding binding affinities. The dataset is divided into an internal dataset (80%) and an external dataset (20%), where the internal dataset is used to train and robust the model performance by employing 5-fold cross validation. The external dataset is used to assess the model's performance.

The performance of the proposed QSAR model is evaluated using two well-known statistical measures; coefficient of determination (R^2) and root mean square error (RMSE). R^2 is used to evaluate the model's fitness and to quantify how much variation in the dependent variable (binding affinity) is explained by the independent variables (features). It ranges between 0 and 1, with higher values indicating better model performance. However, RMSE measures the relative error between the predicted and actual values of binding affinity. To demonstrate the effectiveness of the DTR model, Fig. 4 displays the actual and predicted binding affinity for 12 distinct feature sets.

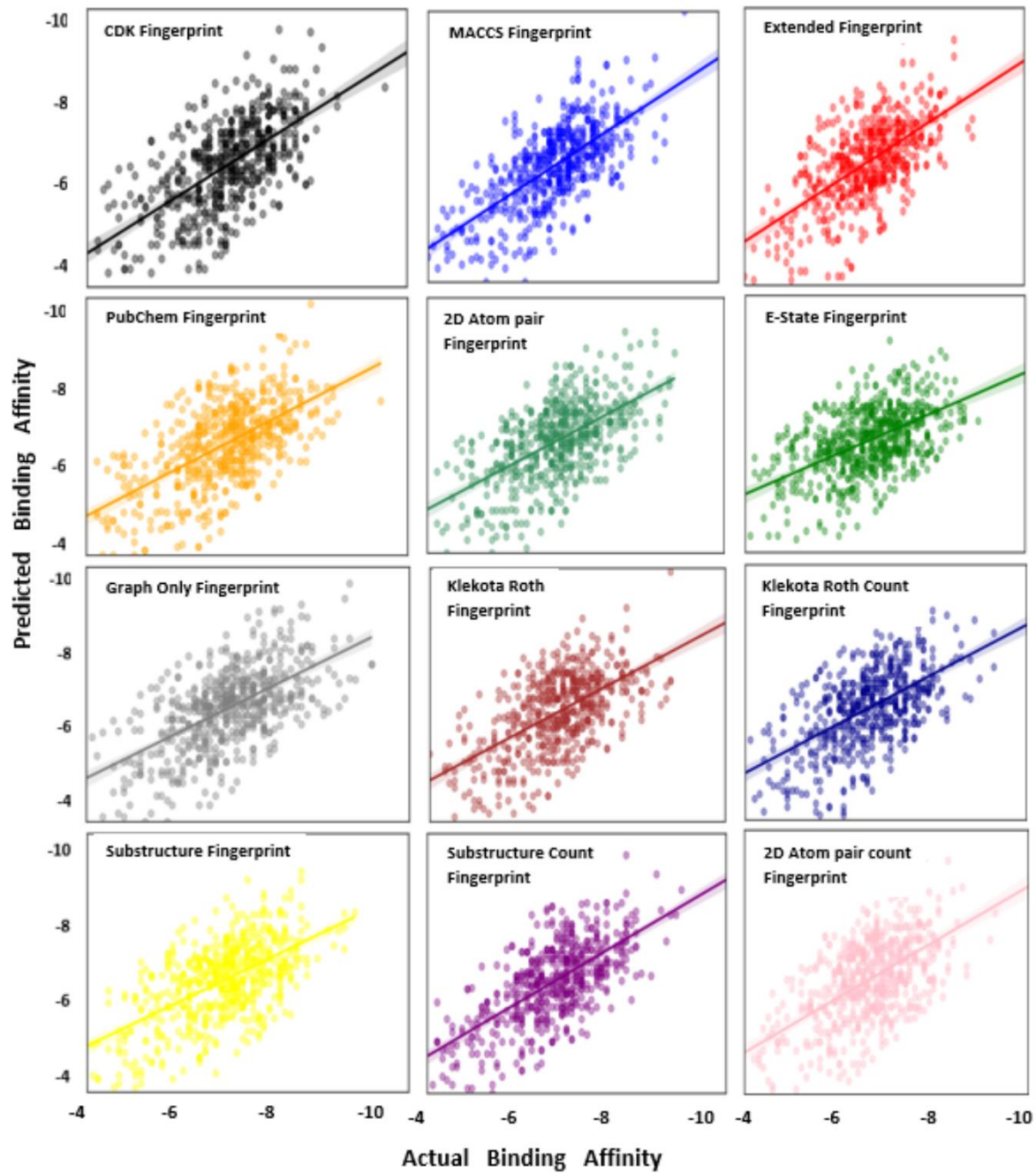


Fig. 4. Scatter plot of 12 feature descriptors for Decision Tree Regression (DTR) model

In this investigation, the effectiveness of the DTR model is analyzed using 12 various feature descriptor sets. The evaluation outcomes, including R^2 , Mean Squared Error (MSE), and Root Mean Squared Error (RMSE) values, are illustrated in Table 2.

Table 2: Performance of DTR Model for Distinct Fingerprints.

Sr. No	Descriptors/ Fingerprints	R^2	MSE	RMSE
1	CDK	0.97	2.81	1.68
2	MACCS	0.97	2.46	1.57
3	Extended CDK	0.90	3.38	1.84
4	PubChem	0.93	3.50	1.87
5	2D Atom pair	0.82	2.91	1.71
6	E-state	0.70	2.70	1.64
7	Graph Only	0.81	2.87	1.69
8	Klekota Roth	0.79	3.27	1.81
9	Klekota Roth count	0.68	3.11	1.76
10	Substructure	0.82	2.85	1.69
11	Substructure count	0.72	2.81	1.68
12	2D Atom pair count	0.83	3.59	1.90

Table 2 presents the performance evaluation of 12 different feature descriptors in predicting the binding affinity of a set of drug compounds. Three performance metrics are used to evaluate the model's performance, namely R^2 , Mean Squared Error (MSE), and Root Mean Squared Error (RMSE). The R^2 metric measures the goodness of fit of the model to the data, where higher values indicate a better fit. The MSE metric calculates the average of the squared differences between the predicted and actual values, while the RMSE metric is the square root of the MSE, and it estimates the error in the same units as the target variable.

The results show that CDK fingerprint and MACCS fingerprint outperformed other fingerprints with an R^2 value of 0.97 and a low RMSE of 1.68 and 1.57, respectively. The PubChem fingerprint also performed well with R^2 value of 0.93 and an RMSE of 1.87. Extended CDK fingerprint, 2D Atom pair fingerprint, E-state fingerprint, Graph only fingerprint, Klekota Roth fingerprint, Klekota Roth count fingerprint, Substructure fingerprint, Substructure count fingerprint, and 2D Atom pair count fingerprint, showed varying degrees of prediction accuracy.

The CDK fingerprint and MACCS fingerprints provide a comprehensive representation of molecular structure and properties. They encode a broad range of chemical features, including substructures, functional groups, and molecular properties. This allows for a holistic characterization of drug molecules, making them suitable for exploring diverse chemical space and identifying potential drug repurposing candidates. Based on these characteristics, CDK fingerprint and MACCS fingerprint are selected for further comparison of our proposed model DTR with other machine learning models. Overall, this table

provides valuable information for selecting the most appropriate feature descriptors for predicting the binding affinity of a set of drug compounds.

3.2. Comparative Analysis

To assess the effectiveness of the proposed QSAR model, a comparison is made with other regression models using two different feature descriptors, namely CDK fingerprint and MACCS fingerprint descriptors. The evaluation of the models is based on two statistical measures of R^2 and RMSE for the external dataset.

Fig. 5 displays a graphical comparison of the actual and predicted binding affinity values using CDK fingerprint feature descriptor for DTR model. The results show that the proposed model DTR outperforms the other models with the highest value of 0.97 of R^2 for the external dataset. This suggests that the model provides a good fit to the data and that the independent variables are strongly associated with the dependent variable.

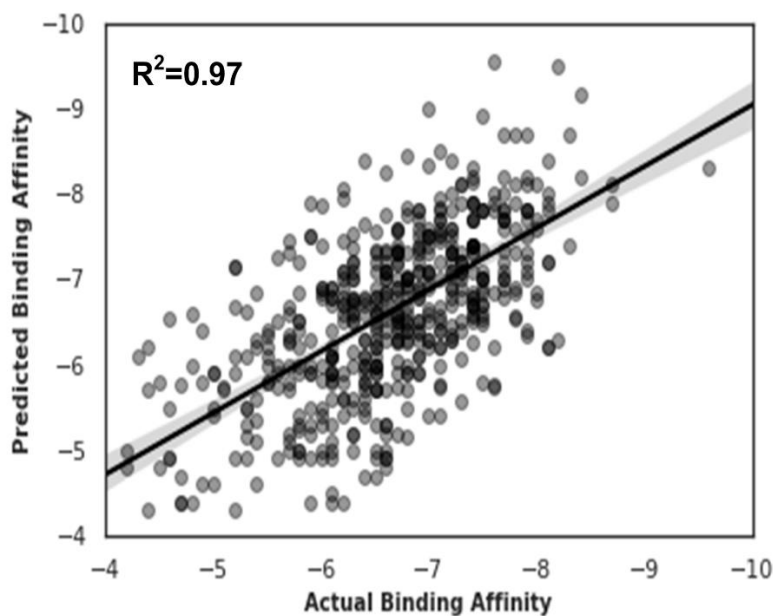


Fig. 5. Regression plot of DTR-QSAR model with CDK fingerprint

The Table in Supplementary File S 1 shows the comparison of the experimental binding affinity of 500 drug compounds of external dataset with their predicted binding affinity using QSAR models including DTR, ETR, GBR, KNNR, MLPR, and XGBR. Each row represents a different drug compound, identified by its Zinc ID in the second column. Third column shows the actual binding affinity of the drug compound, while the remaining columns show the predicted binding affinity of the compound using the different ML regression models. Fifth column shows the difference between the actual and predicted binding affinity using DTR model with mean absolute difference (MAD) of 0.54, while seventh and ninth columns show the MAD values 0.59 for ETR and GBR model. However, the eleventh, thirteen, and the fifteen columns show MAD values 0.80, 0.80, and 0.68 for KNNR, MLPR, and XGBR models, respectively.

The differences between the actual and predicted binding affinity values in each column provide an indication of the accuracy of each model in predicting the binding affinity of the drug compounds. At the end, the analysis of MAD reveals that proposed DTR model has more accuracy with minimum value of 0.09 in predicting the binding affinities of drug compounds with the specific target protease.

The proposed DTR model is also compared with other regression models, using MACCS fingerprint descriptors, to evaluate their performances on the external dataset using R^2 and RMSE measures. Fig. 6 presents a graphical description of DTR model using MACCS fingerprint feature descriptors. The results indicated that proposed DTR model outperformed the other regression models, with the highest R^2 value of 0.97 for the external dataset. This signifies that the model explained a large proportion of the variance in the dependent variable based on the given set of independent variables, even though the relationship between the variables may not be strictly linear.

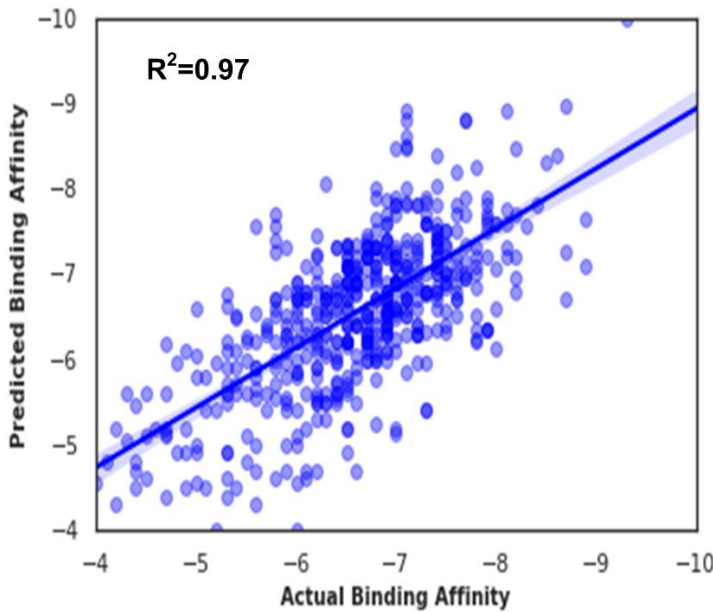


Fig. 6. Regression plots of R^2 using MACCS fingerprint features for external dataset

Table 3 highlights the performance comparison of DTR model with other regression models on two different feature sets, CDK Fingerprint and MACCS Fingerprint in terms of R^2 , and RMSE values. The DTR achieved R^2 value of 0.97 with RMSE value of 1.68 for CDK Fingerprint feature set. For MACCS Fingerprint feature set, DTR model has obtained the R^2 value of 0.97, and the RMSE value of 1.57. However, ETR and KNNR models have obtained relatively lower performance for both feature sets. MLPR and XGBR showed poor fit with lower R^2 and higher RMSE values for both feature sets. Overall, quantitative results suggest that DTR is more suitable choice for predicting the binding affinity for both CDK Fingerprint and MACCS Fingerprint feature sets.

Table 3: Performance Comparison of QSAR Regression Models.

Regression Model	CDK Fingerprint		MACCS Fingerprint	
	R^2	RMSE	R^2	RMSE

DTR	0.97	1.68	0.97	1.57
ETR	0.91	1.85	0.85	1.80
KNNR	0.90	1.84	0.96	1.86
GBR	0.87	1.83	0.88	1.81
MLPR	0.70	1.74	0.60	1.64
XGBR	0.60	1.87	0.54	1.85

3.3. Molecular Docking

Our main objective was to determine the effectiveness of the selected drug molecules in interacting with the target protease. For this purpose, molecular docking technique used to predict and analyze the interactions between ligand and target protease. It helps in understanding the binding affinity and the orientation of ligands within the protease active site. In our study, we used a ligand-based docking approach to evaluate the binding affinities of drug molecules extracted from the Zinc database, as described in Section 3.1.3. The drug molecules were converted into PDBQT format and their binding affinities with the target protein 7JSU were evaluated in kcal/mol units.

Fig. 7 A displays the binding pocket of the target protease 7JSU. On the other hand, Fig. 7 B shows the 3D interaction view of complex of 7JSU with ligand 2297 bound with it. This figure depicts the interacting residues of 7JSU with ligand 2297 atoms along with intermolecular distances. In this interaction, hydrogen bonds are represented by dotted lines shown in green color. A hydrogen bond occurs when a hydrogen atom from the protein interacts with an electronegative atom (such as oxygen or nitrogen) from the ligand or vice versa. The distance between the hydrogen donor and the acceptor atom is around 2-3 Å. The distance shows values in the range of 2.36 -2.51 Å for hydrogen bonds. These shorter distances suggest that the hydrogen bond interactions between the protein and ligand are relatively strong and stable. The detail numerical description about the hydrophobic interaction and the H-bonding is provided in the next section. These tables focuses the protein-ligand structural context of hydrophobic contacts, hydrogen bonds, and atomic coordination. These useful information characterize the structural and energetic aspects of the protein-ligand complex.

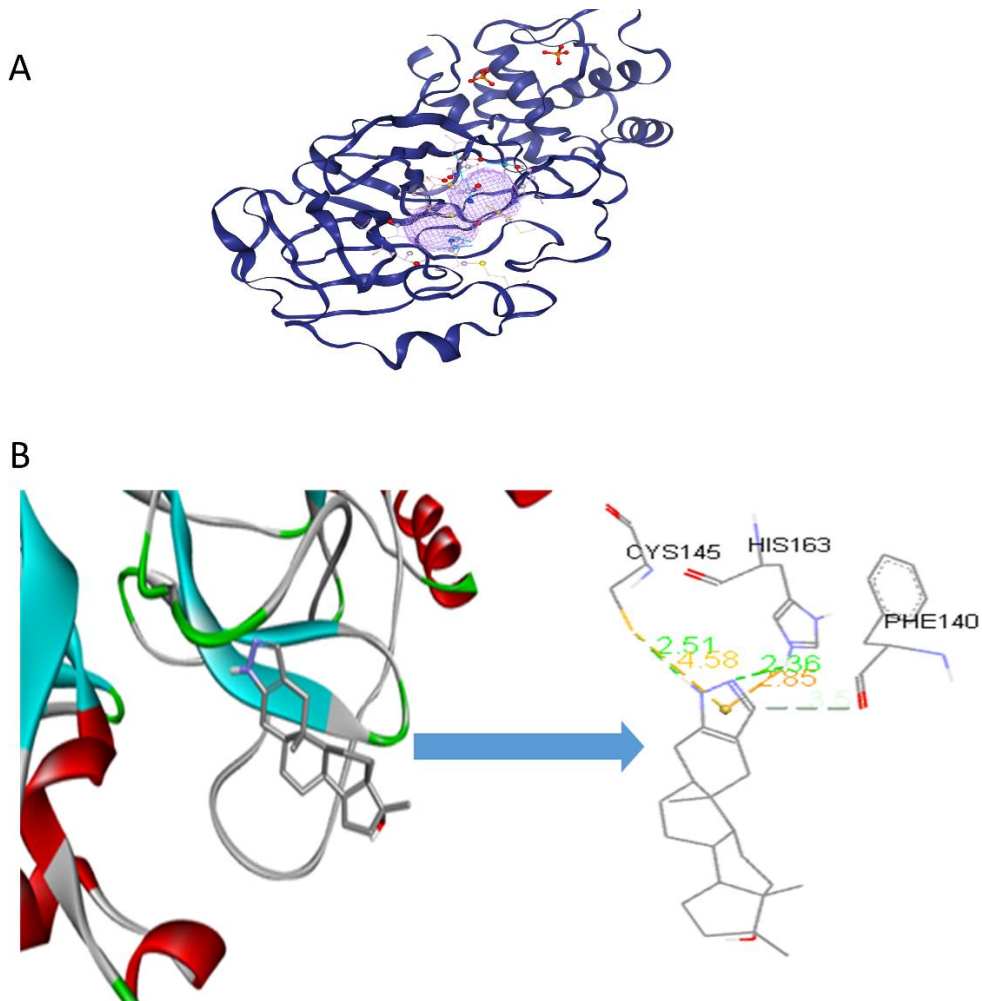
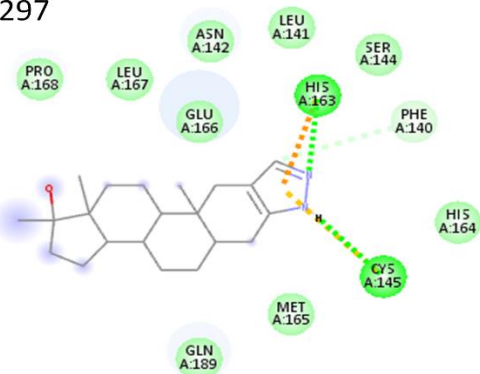


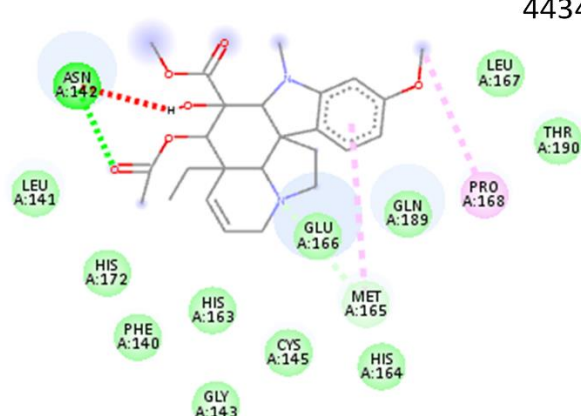
Fig. 7. (A)- The binding pocket of the target protease 7JSU; (B)- 3D interaction view of Protein- ligand ID 2297 Complex.

Fig. 8 demonstrates the 2D view of optimal poses of six top rank drug compounds interacting with the target protease corresponds to the best binding affinity. These drug molecules have the best binding affinities ranging from -15.1 to -13.6 kcal/mol. The optimal pose refers to the specific orientation and conformation of the ligand molecule that achieves the lowest binding affinity with the target protease. The most negative binding energy value represents the best ligand pose towards the target. 2D view show the interaction of protein-ligand in terms of Van Der Waals, conventional hydrogen bond, carbon hydrogen bond, Pi-cation, Pi-sulfur, Pi-Pi T-shaped, unfavorable donor-donor, alkyl, Pi-alkyl. These different types of interactions play important roles in the overall stability of protein-ligand binding.

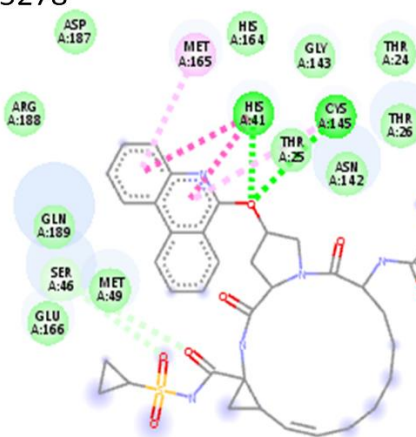
2297



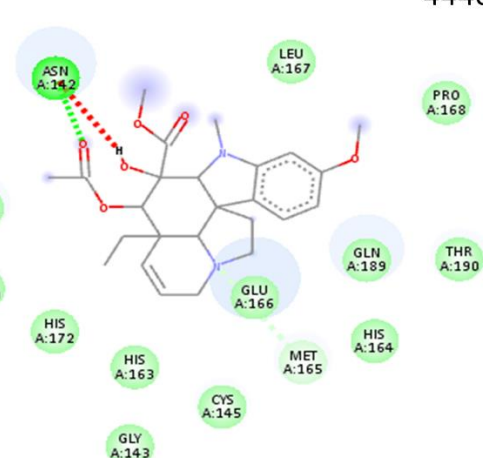
4434



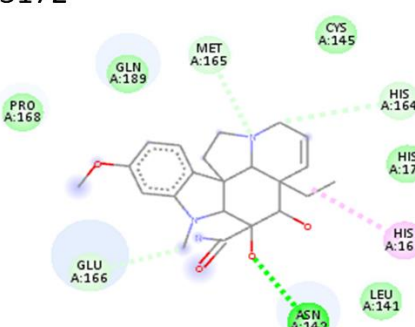
5278



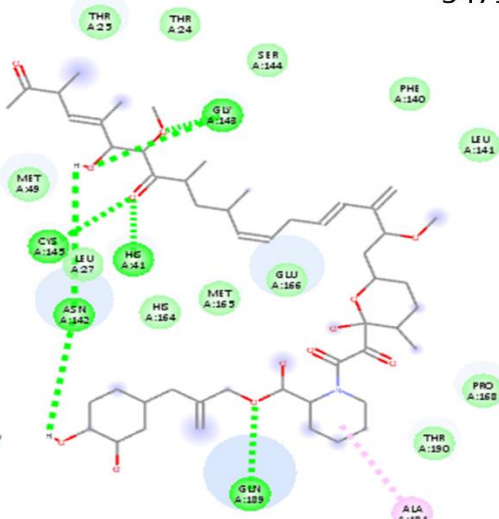
4440



3172



5471

**Interactions**

van der Waals	Pi-Cation	Unfavorable Donor-Donor
Conventional Hydrogen Bond	Pi-Sulfur	Alkyl
Carbon Hydrogen Bond	Pi-Pi T-shaped	Pi-Alkyl

Fig. 8. The optimal poses (2D view) of six top rank drug compounds interacting with target protease 7JSU

On the other hand, docking accuracy is evaluated by measuring the root-mean-square deviation (RMSD) of the ligand molecule from its initial position in the protease complex. A lower RMSD value indicates a superior docking geometry of the ligand molecule. Interestingly, our analysis demonstrates that all six ligands achieved an RMSD value of zero at their optimal poses, implying a high level of accuracy in the docking geometry. Table 4 shows the binding affinities (BA) values of the six top-ranked drug molecules and the corresponding amino acid (AA) residues involved in the hydrophobic interaction and H-bonding. The ligands 2297, 4434, 5278, 4440, 3172, and 5471 have obtained the best BA values -15.1, -14.4, -14.4, -13.9, -13.6, and -13.6 kcal/mol, respectively. This table shows that ligand 2297, with minimum -15.1 kcal/mol, is the most promising drug compound.

The analysis of ligand poses and their corresponding binding energies helps establish a relationship between the molecular structure of the ligands and their binding affinity. It indicates the strong interaction and potential efficacy of the ligand molecule as a drug candidate. The identified amino acids involved in hydrophobic interactions and hydrogen bonds provide valuable insights into the molecular mechanisms underlying ligand-protein interactions. Further, exploration and analysis of these interactions would contribute to the development of novel therapeutic strategies targeting the specific residues and improving the efficacy of drug candidates.

Table 4: Top Ranked Six Ligands with Target Protein 7JSU.

Sr. No.	Zinc ID	Ligand ID	BA (kcal/mol)	List of AA Residues	
				Hydrophobic interaction	H-bonding
1	ZINC3873365	2297	-15.1	GLU166	HIS163
2	ZINC85432544	4434	-14.4	PHE140, ET165, GLU166	ASN142, GLU166, GLN189
3	ZINC203757351	5278	-14.4	MET165, GLU166, GLN189	THR26, HIS41, ASN119
4	ZINC85536956	4440	-13.9	PHE140, LEU141, MET165, GLU166	ASN142, GLU166, GLN189
5	ZINC8214470	3172	-13.6	PHE140, GLU166	ASN142, GLU166
6	ZINC261494640	5471	-13.6	GLU166, GLN189	HIS41, ASN142, GLY143, GLN189

3.3.1. Hydrophobic Interactions

Table 5 provides the hydrophobic Interactions between C-H bonds of six ligands with the chain A of 3CL target protein. Due to non-polar nature, the residues MET, PHE, GLU, GLN, and LEU exhibited the hydrophobic interactions. It is worth noting that these hydrophobic residues are buried within the protein core. The large side chain based hydrophobic residues (MET, PHE, GLU, GLN, and LEU) contribute significantly to the formation of the protein's hydrophobic core, which plays a crucial role in maintaining the stability of the ligand-protein structure.

In this table, ligand 2297 exhibits a hydrophobic interaction with residue GLU166A, where a relatively smaller intermolecular distance of 3.22 Å is found between protein atom at position 1578 and ligand atom at position 2889. However, Ligand 3172 give interactions with two amino acid residues of PHE140 and GLU166 with intermolecular distances of 3.62 Å and 3.50 Å, respectively. Furthermore, this table

reveals hydrophobic interactions with other ligands 4434, 4440, 5278, and 5471 with residues MET, PHE, GLU, GLN, and LEU. These Hydrophobic interactions are characterized by varying intermolecular distances ranging from 3.42 Å to 3.95 Å.

Table 5: Hydrophobic Interactions of Top Ranked Six Ligands with the Target Protease.

Ligand ID	Index	AA Residue	Distance (Å)	Ligand Atom	Protein Atom
2297	1	GLU166(A)	3.22	2889	1578
3172	1	PHE140(A)	3.62	2897	1336
	2	GLU166(A)	3.50	2897	1578
4434	1	PHE140(A)	3.94	2892	1336
	2	MET165(A)	3.60	2890	1569
	3	GLU166(A)	3.06	2892	1578
4440	1	PHE140(A)	3.89	2892	1336
	2	LEU141(A)	3.95	2869	1351
	3	MET165(A)	3.73	2884	1569
	4	GLU166(A)	3.06	2892	1578
5278	1	MET165(A)	3.42	2909	1569
	2	GLU 166(A)	3.82	2905	1578
	3	GLN 189(A)	3.76	2912	1788
	4	GLN 189(A)	3.59	2871	1787
5471	1	GLU 166(A)	3.92	2905	1578
	2	GLN 189(A)	3.83	2913	1788

3.3.2. H-bonding Interaction

H-bond is a type of intermolecular bond that occurs between H-atom bonded to electronegative N or O atoms. The acceptor N atom within a protein possesses a lone pair of electrons, which interact with H atom from the ligand and vice versa. The donor atom within molecule donates the H-bond. The H-bonds are weaker than covalent bonds. The H-bond interaction analysis help to understand the structural and geometrical stability of protein ligand interaction and to improve the physiochemical and drug biological process. The polar and charged residues in their side chains at different positions such as ASN142, GLU166, THR26, HIS163, and GLY143, etc. The polar residues ASN, GLU, GLN, and THR donate or accept H-bond. The residue His has two-NH groups in the side chains, depending on the environment and pH level, can be polar. The residues ARG, LYS and TRP possess N donor atom in their side chains. On the other hand, the residues ASP and GLU are H-bond acceptor (O) atom in side chain.

In the ligand molecules and AA residue combination, the distances H-acceptor and donor-acceptor play a significant role in determining the strength of hydrogen bonds. The smaller distances indicate the stronger H-bonds, as the electrostatic interaction between the partially positive hydrogen and the partially negative acceptor atom is stronger when they are closer together. We compared the values of these distances and analyzed to understand the strength of H-bonding interactions. The optimal (higher) donor

angle of each residue is crucial in assessing the strength or weakness of hydrogen bonding. The donor angle represents the spatial orientation of the donor atom involved in the hydrogen bond. The angle influences the alignment and stability of the hydrogen bond, impacting its strength. A more favorable and optimal values of the donor angles results in stronger H-bonds, while deviations from the ideal angle (180) can weaken the interaction. Moreover, the protein donor and acceptor atoms also contribute to the strength of H-bond. These donor and acceptors atoms affect the overall stability and specificity of the hydrogen bonds formed in ligand protein interaction.

The Table 6, highlights the useful values of the H-acceptor distances and donor-acceptor distance, the donor angle, the donor atom, and acceptor atom. These values are focusing on H-A and D-A distances, donor angle, and protein donor/acceptor atoms. The numerical distance values between specific atoms involved in the hydrogen bonding interactions, are given in angstroms (Å). The "Distance H-A" and "Distance D-A" measures represent the "H-Acceptor" distance and "Donor-Acceptor" distance, respectively. These distances provide valuable information about the proximity of the atoms in the hydrogen bond. Their numerical values highlight the strength and geometry of H-bonding interactions in protein-ligand complexes. The specific values of these distances vary depending on the nature of donor and acceptor molecules. The smaller distances indicate the stronger H bonds, which improve the stability of the ligand protein interaction.

For ligand ID 2297, the residue HIS163 forms H-bond with donor angle of 136.68 degrees using the acceptor ligand. The bond is formed between the N+ atoms of the donor protein at 1548 position with N atom of the acceptor at 2887 position. The proximity of the H-acceptor distance (2.36 Å) and donor-acceptor distance (3.18 Å) is significant, as the smaller distances indicate the existing of stronger hydrogen bonds for ligand ID 2297. However, for ligand 3172, the ASN142 participates in hydrogen bonding with a donor angle of 120.04 degrees. The donor angle is favorable for the hydrogen bond, enhancing its stability. The H-bond is formed between the protein/donor N atom at position 1359 and the ligand/acceptor oxygen atom at 2893. This introduces more interaction with potential variations in the bonding patterns. For ligand 3172, the optimal smaller values of H-acceptor (3.17 Å) and donor-acceptor (3.78 Å) distances indicate a stronger hydrogen bond.

Similarly, for ligand ID 4434, the residue ASN142 form a donor angle of 122.86 degree with the ligand acceptor. The H-bond is formed between the donor N atom at position 1359 and the ligand/acceptor oxygen atom at 2893 potentially leading to a more diverse hydrogen bonding network. The distances values (2.56 Å and 3.23 Å) of H-acceptor and donor-acceptor signify a hydrogen bond. The donor angle of 122.86 degrees, although different from the ideal 180 angle, still contributes to the stability of the hydrogen bond.

Continuing to ligand ID 4440, the H bond of the residue ASN142 is more significant as compared to residues GLU166, GLN189, and THR26. This residue has a smaller H-acceptor distance of 2.51 Å with larger donor-acceptor distance 4.04 Å. This donor angle contributes to the stability and strength of the hydrogen bond, as it aligns the donor and acceptor atoms optimally. The increased donor angle up to 155.73 degree contribute more to the geometrical stability of the H bond. H-bond is formed between the donor atom at 1359 [Nam] and the ligand/acceptor atom at 2898 [O2]. Finally, for ligand ID 5278, the residue THR26 has optimal donor angle of 147.66 degree. The H-bond is formed between the protein donor nitrogen atom at position 224 and the acceptor oxygen atom at position 2889. For this ligand

relatively larger distances value 4.07 Å of donor-acceptor help to decrease donor angle up to 147.66 degree, although deviating from the ideal angle (180 degree), still contributes to the stability of the hydrogen bond.

Table 6: H-bonds of Top Ranked Six Ligands with the Target Protease.

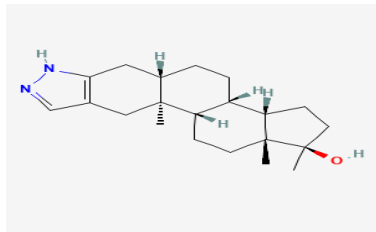
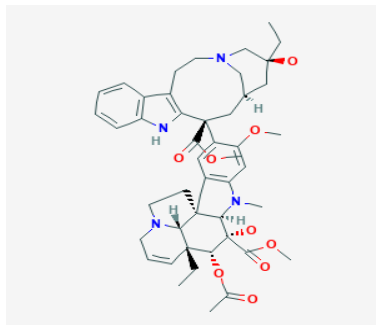
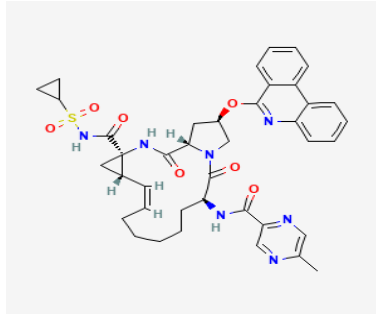
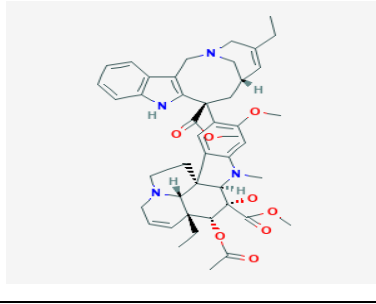
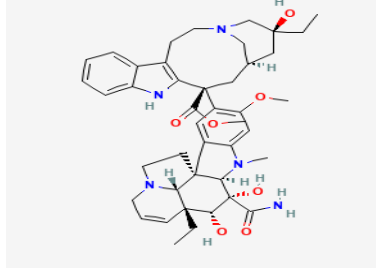
Ligand ID	Index	AA Residue	Distance (Å) H-A D-A	Donor Angle	Protein donor	Side chain	Donor Atom	Acceptor Atom
2297	1	HIS163(A)	2.36 3.18	136.68	Yes	Yes	1548 [Npl]	2887 [N2]
	1	ASN142(A)	3.17 3.78	120.04	Yes	Yes	1359 [Nam]	2893 [O2]
3172	2	GLU166(A)	2.76 3.61	140.74	Yes	No	1574 [Nam]	2876 [N3]
	3	GLU166(A)	2.43 3.36	159.55	No	Yes	2890 [Nam]	1582 [O-]
4434	1	ASN142(A)	2.56 3.23	122.86	Yes	Yes	1359 [Nam]	2893 [O3]
	2	ASN142(A)	2.48 3.30	136.86	Yes	No	1353 [Nam]	2870 [O2]
	3	GLU166(A)	3.01 3.65	121.92	Yes	No	1574 [Nam]	2877 [N3]
	4	GLN189(A)	3.45 3.80	102.50	Yes	Yes	1790 [Nam]	2899 [O3]
4440	1	ASN142(A)	3.09 3.37	140.66	Yes	No	1353 [Nam]	2870 [O2]
	2	ASN142(A)	2.51 4.04	155.73	Yes	Yes	1359 [Nam]	2898 [O2]
	3	GLU166(A)	2.97 3.61	121.57	Yes	No	1574 [Nam]	2877 [N3]
	4	GLN189(A)	3.51 3.86	102.95	Yes	Yes	1790 [Nam]	2893 [O3]
5278	1	THR26(A)	3.17 4.07	147.66	Yes	No	224 [Nam]	2889 [O2]
	2	HIS41((A))	2.54 3.28	129.13	Yes	Yes	380 [Npl]	2899 [O3]
	3	ASN119(A)	1.99 2.97	160.52	Yes	Yes	1147 [Nam]	2920[Nam]
5471	1	HIS41(A)	1.87 2.74	139.95	Yes	Yes	380 [Npl]	2918 [O2]
	2	ASN142(A)	2.93 3.45	113.86	No	Yes	2931 [O3]	1360 [O2]
	3	ASN142(A)	2.91 3.73	138.46	Yes	Yes	1359 [Nam]	2875 [O3]
	4	ASN142(A)	2.36 3.18	139.18	No	Yes	2875 [O3]	1360 [O2]
	5	GLY143(A)	1.92 2.93	170.34	Yes	No	1364 [Nam]	2920 [O3]
	6	GLN189(A)	2.43 3.26	138.41	Yes	Yes	1790 [Nam]	2893 [O2]

3.4. Physiochemical analysis of drug candidates

On the basis of our analysis, we shortlisted six drug compounds having more efficacy and strong interaction with specific target protease 3CLpro. Table 7 provides a detailed description of these six drug compounds having the lowest binding energies. The description includes the Zinc ID, molecular formula, SMILES, and 2D structure of the drug compounds.

Table 7: Description of Top Ranked Six Drug Compounds.

Zinc ID	Molecular Formula	SMILES	2D Structure
---------	-------------------	--------	--------------

ZINC3873 365	C21H32N2O	<chem>C[C@]12Cc3cn[nH]c3C[C@@H]1CC[C@H]1[C@@H]2CC[C@]2(C)[C@H]1CC[C@@]2(C)O</chem>	
ZINC8543 2544	C46H58N4O9	<chem>CC[C@]1(O)C[C@@H]2CN(CCc3c([nH]c4cccc34)[C@@@](C(=O)OC)(c3cc4c(cc3OC)N(C)[C@H]3[C@@]1(O)(C(=O)OC)[C@H](OC(C)=O)[C@]5(CC)C=CCN6CC[C@]43[C@@H]65)C2)C1</chem>	
ZINC2037 57351	C40H43N7O7S	<chem>Cc1cnc(C(=O)N[C@H]2CCCCC/C=C\[C@H]3C[C@@]3(C(=O)NS(=O)(=O)C3CC3)NC(=O)[C@@H]3C[C@@H](Oc4nc5cccc5c5cccc45)CN3C2=O)cn1</chem>	
ZINC8553 6956	C45H54N4O8	<chem>CCC1=C[C@H]2CN(C1)Cc1c([nH]c3cccc13)[C@@@](C(=O)OC)(c1cc3c(cc1OC)N(C)[C@H]1[C@@@](O)(C(=O)OC)[C@H](OC(C)=O)[C@]4(CC)C=CCN5CC[C@]31[C@@H]54)C2</chem>	
ZINC8214 470	C43H55N5O7	<chem>CC[C@]1(O)C[C@H]2CN(CCc3c([nH]c4cccc34)[C@@@](C(=O)OC)(c3cc4c(cc3OC)N(C)[C@H]3[C@@]1(O)(C(N)=O)[C@H](O)[C@]5(CC)C=CCN6CC[C@]43[C@@H]65)C2)C1</chem>	

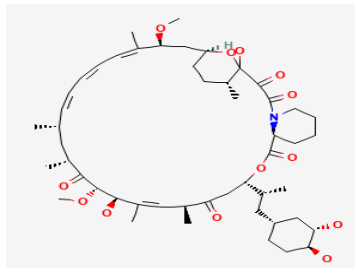
ZINC2614 94640	C50H77NO13	<chem>CO[C@H]1C[C@H]2CC[C@H](C)[C@H](O)(O2)C(=O)C(=O)N2CCCC[C@H]2C(=O)O[C@H]([C@H](C)C[C@H]2CC[C@H](O)[C@H](O)C2)CC(=O)[C@H](C)/C=C(/C)[C@H](O)[C@H](O)C(=O)[C@H](C)C[C@H](C)/C=C/C=C/C=C\1C</chem>	
-------------------	------------	---	---

Table 8 provides few selected physicochemical properties of six potential drug candidates represented by their Zinc ID, molecular weight, logP, hydrogenbond donors and acceptors, number of rings, heavy atoms, heteroatoms, and fraction sp3. These properties play critical role in the efficacy and bioactivity of the drug compounds. These properties are important in drug discovery as they provide insights into the potential efficacy and pharmacokinetic profile of a drug.

The analysis of these physicochemical properties of drug molecules is necessary to understand their behavior in biological systems and predict their efficacy and safety. In this study, we have selected physicochemical properties of drugs, such as molecular weight (Mol.Wt), LogP, rings, hydrogenbond donors (HBD), hydrogenbond acceptors (HBA), heavy atoms, heteroatoms, and sp3 fraction, play a critical role in determining their binding affinity to a specific target protease. For example, molecular weight is a key factor in determining the pharmacokinetics and pharmacodynamics of drugs, as well as their ability to cross cell membranes and interact with target proteases. It has been observed that compounds having optimal molecular weight have a higher chance of binding to target proteases. Similarly, logP, or the logarithm of the partition coefficient, is another important factor that affects drug binding affinity. A high logP value indicates that the drug is more lipophilic and is more likely to interact with hydrophobic regions of the protease. A study (Tsantili-kakoulidou and Demopoulos, 2021) found that logP was a significant factor in predicting the binding affinity of small molecule drugs with target. In the context of drug-protein interactions, HBD and HBA contribute to the formation of specific molecular interactions that are essential for binding and recognition. The number of rings in a drug molecule is another important property related to binding affinity and selectivity for specific targets. The drug compounds with two or three rings have a higher likelihood of exhibiting good oral bioavailability and target affinity, while excessively large or complex rings can interfere with binding or increase toxicity (Lipinski et al., 2012). The presence of heavy atoms and heteroatoms, particularly nitrogen and oxygen, can significantly affect drug-target interactions by forming hydrogen bonds or other electrostatic interactions with target residues. However, too many or too few heteroatoms can disrupt drug solubility, membrane permeability, and other properties critical to bioavailability.

The key property the sp3 fraction of a drug compound has been shown to influence its physicochemical properties and target affinity (Leeson et al., 2021). The sp3 fraction represents the percentage of carbon atoms with three or more single bonds. The higher sp3 fractions are associated with increased water solubility, lower toxicity, and improved pharmacokinetic properties, while excessively low values can lead to poor bioavailability or reduced target selectivity.

Table 8: Physicochemical Properties of Selected Drug Compounds.

Sr. No	Zinc ID	Mol. Wt (g/mol)	LogP	Rings	HBD, HBA	Heavy Atoms	Hetero Atoms	Fraction sp3
1	ZINC3873365	328.5	4.118	5	2, 2	24	3	0.86
2	ZINC85432544	810.9	3.99	9	5, 10	59	13	0.59
3	ZINC203757351	765.8	3.637	8	3, 10	55	15	0.42
4	ZINC85536956	778.9	4.754	9	4, 9	57	12	0.53
5	ZINC8214470	753.9	2.732	9	7, 8	55	12	0.58
6	ZINC261494640	900.1	5.527	4	4, 10	64	14	0.74

Molecular weight is an important factor as it affects the solubility, bioavailability, and transport of a drug in the body. In the table, the molecular weight of these drugs ranges from 328.5 g/mol to 914.1 g/mol, indicating that the drugs vary widely in size. We observed that the drugs with higher molecular weight tended to have a higher number of heavy atoms and heteroatoms. This suggests that larger molecules may be more effective in binding to specific targets. However, we also observed that some of the drugs with lower molecular weight have a higher fraction sp3, which may indicate a greater degree of three-dimensional complexity and potentially better binding interactions. Further, the lipophilicity of the drugs, as measured by their logP values, ranges from 2.456 to 6.181, with most of the drugs having a logP value between 3 and 5. Lipophilicity is important in drug development as it can impact drug absorption, distribution, metabolism, and excretion (ADME) properties. Furthermore, most of the values for HBD are ≥ 4 and HBA are ≥ 8 in this table. Having more HBD and HBA in a drug molecule increases its ability to form multiple hydrogen bonds with the protein's binding site. This can enhance the interactions and contribute to stronger binding affinity.

This table shows that the number of rings in the molecules varies from 4 to 10, with a majority of the drugs having 6 or more rings. The heavy atom count ranges from 24 to 65, indicating a moderate to high number of non-hydrogen atoms in the drug molecules. The number of rings and heavy atoms in a molecule can affect its stability, potency, and specificity. Molecules with a larger number of rings and heavy atoms are often more complex and may have a higher probability of interacting with the target receptor.

This table indicates the number of heteroatoms in the drugs ranges from 3 to 15, with most of the drugs having between 12 and 15 heteroatoms. These values are important because they can provide insights into the potential binding interactions between the drug and its target. The fraction sp3 is another key property which represents the proportion of carbon atoms in the drug that are sp3 hybridized, ranges from 0.42 to 0.90. The most of the drugs having a fraction sp3 value greater than 0.50. A higher fraction sp3 value indicates that a drug has a higher degree of 3D character that can be beneficial for binding to certain targets.

Overall, these physicochemical properties of selected six drugs play a critical role in drug discovery and development, and their understanding. These properties are essential for designing drugs with improved

efficacy and pharmacokinetic properties. These drug compounds have the potential for repurposing for the treatment of various diseases. These physicochemical properties would be helpful in further *vitro* and *in vivo* studies that are necessary to determine the efficacy, safety, and dosage of these drugs for the treatment of specific diseases. This useful analysis of these drugs provides a starting point for drug repurposing research. This highlights the importance of considering the physicochemical properties of the drugs for repurposing purposes. The potential drug candidates that we suggest to repurpose against COVID-19 3CL protease are described with their generic name ID and original purpose in Table 9.

Table 9: Repurposed proposed drugs in the study

Sr. No.	Zinc ID	Generic Name	Original Purpose/ Treatment	New Indication
1	ZINC3873365	Stanozolol	Hereditary angioedema (HAE), anemia, and some types of breast cancer.	COVID-19 3CL
2	ZINC85432544	Vinblastine	Breast cancer, testicular cancer, neuroblastoma, Hodgkin's and non-Hodgkin's lymphoma, mycosis fungoides, histiocytosis, and Kaposi's sarcoma.	COVID-19 3CL
3	ZINC203757351	Paritaprevir	Antiviral agent for Hepatitis C Virus (HCV) infections.	COVID-19 3CL
4	ZINC85536956	Vinorelbine tartrate	Non-small cell lung cancer, locally advanced or spread to other parts.	COVID-19 3CL
5	ZINC8214470	Vindesine	Acute leukaemia, malignant lymphoma, Hodgkin's disease, acute erythraemia and acute panmyelosis	COVID-19 3CL
6	ZINC261494640	41-O-demethyl rapamycin	Tumor-based cancers, prevent organ rejection in kidney transplant patients, and coat stents implanted in heart disease patients	COVID-19 3CL

4 Conclusion

In this work, we conducted a comprehensive study to repurpose FDA-approved drugs. We developed a computational framework using molecular docking and machine learning approaches to identify potential therapeutics for COVID-19 targeting the main protease 3CL of SARS-CoV-2. Out of 5903 world-approved including FDA-approved drugs, we identified six drugs with high binding affinity and favorable binding energies. To improve the efficiency of drug repurposing approach, we modeled the binding affinities using several well-known ML-based regression algorithms. The results demonstrated that DTR model have improved statistical measures of R^2 and RMSE values as compared to other regression models. Further, DTR model has performed better on ten feature descriptors and outperformed on other two feature descriptors (CDK and MACCS). The CDK fingerprint and MACCS fingerprint are selected based on their ability to comprehensively represent molecular structure and properties,

interpretability, and computational efficiency. These characteristics make them suitable for our study's goal of exploring drug repurposing potential. This highlights that DTR model, with improved statistical measures, is most suitable in predicting the binding affinity as compared to other regression models. Further, we analyzed the physiochemical properties of the shortlisted compounds with respect to binding interaction to specific target. This revealed that selected compounds are more effective to inhibit the viral enzyme 3CLpro of COVID-19.

Overall, our study provides a valuable contribution in the field of drug repurposing to accelerate the identification of potential therapeutic candidates. We believe that our novel drug findings using in-silico research based approach are useful in the fight against COVID-19. However, more research is needed to validate the efficacy and safety of these drugs in clinical trials.

Supplementary Materials: The Supplementary file (Supplementary File S 1) consists of a table provided comparison of the regression models in predicting binding affinities with a total of 500 drug compounds.

Funding: This research did not receive any specific grant from funding agencies in the public, commercial, or not-for-profit sectors.

Conflicts of Interest: There are no conflicts of interest to declare by the authors.

References:

Adedayo, A., Famuti, A., 2023. Informatics in Medicine Unlocked In-silico studies of Momordica charantia extracts as potential candidates against SARS-CoV-2 targeting human main protease enzyme (M pro). *Informatics in Medicine Unlocked* 38, 101216.

Ahmed, A., Abdusalam, A., Murugaiyah, V., 2020. Identification of Potential Inhibitors of 3CL Protease of SARS-CoV-2 From ZINC Database by Molecular Docking-Based Virtual Screening. *Frontiers in molecular biosciences* 419. <https://doi.org/10.3389/fmolb.2020.603037>

Aqeel, I., Bilal, M., Majid, A., Majid, T., 2022. Hybrid Approach to Identifying Druglikeness Leading Compounds against COVID-19 3CL Protease. *Pharmaceuticals* 15, 1333.

Boyle, N.M.O., Banck, M., James, C.A., Morley, C., Vandermeersch, T., Hutchison, G.R., 2011. Open Babel : An open chemical toolbox. *Journal of Cheminformatics* 3, 1–14.

Elmezayen, A.D., Al-obaidi, A., Şahin, A.T., Yelekçi, K., 2021. Drug repurposing for coronavirus (COVID-19): in silico screening of known drugs against coronavirus 3CL hydrolase and protease enzymes. *Journal of Biomolecular Structure and Dynamics* 39, 2980–2992. <https://doi.org/10.1080/07391102.2020.1758791>

Ghosh, N., Saha, I., Gambin, A., 2023. Interactome-Based Machine Learning Predicts Potential Therapeutics for COVID-19. *ACS Omega*. <https://doi.org/10.1021/acsomega.3c00030>

Infections, C.-, Ng, T.I., Correia, I., Seagal, J., Degoey, D.A., Schrimpf, M.R., Hardee, D.J., Noey, E.L., Kati, W.M., 2022. Antiviral Drug Discovery for the Treatment of COVID-19 Infections. *Viruses* 14, 961.

Irwin, J.J., Tang, K.G., Young, J., Dandarchuluun, C., Wong, B.R., Khurelbaatar, M., Moroz, Y.S., May, J., Sayle, R.A., 2020. ZINC20 □ A Free Ultralarge-Scale Chemical Database for Ligand Discovery.

Journal of Chemical information and Modeling 60, 6065–6073.
<https://doi.org/10.1021/acs.jcim.0c00675>

Jha, N., Prashar, D., Rashid, M., Shafiq, M., Khan, R., Pruncu, C.I., Tabrez Siddiqui, S., Saravana Kumar, M., 2021. Deep Learning Approach for Discovery of in Silico Drugs for Combating COVID-19. *Journal of Healthcare Engineering* 2021, 1–13. <https://doi.org/10.1155/2021/6668985>

Jin, Z., Du, X., Xu, Y., Deng, Y., Liu, M., Zhao, Y., 2020. Structure of M pro from SARS-CoV-2 and discovery of its inhibitors. *Nature* 582, 289–293. <https://doi.org/10.1038/s41586-020-2223-y>

Khan, N., Muzammil, K., Alshahrani, A.M., 2023. In-silico approaches for identification of compounds inhibiting SARS-CoV-2 3CL protease. *PloS one* 18, 1–27. <https://doi.org/10.1371/journal.pone.0284301>

Leeson, P.D., Bento, A.P., Gaulton, A., Hersey, A., Manners, E.J., Radoux, C.J., Leach, A.R., 2021. Europe PMC Funders Group Target-based evaluation of ‘drug-like’ properties and ligand efficiencies. *Journal of Medicinal Chemistry* 64, 7210–7230. <https://doi.org/10.1021/acs.jmedchem.1c00416.Target-based>

Lipinski, C.A., Lombardo, F., Dominy, B.W., Feeney, P.J., 2012. Experimental and computational approaches to estimate solubility and permeability in drug discovery and development settings i. *Advanced Drug Delivery Reviews* 64, 4–17. <https://doi.org/10.1016/j.addr.2012.09.019>

Mateen, A., Farooq, S., Ullah, A., Choudhary, M.I., 2023. International Journal of Biological Macromolecules Repurposing of US-FDA approved drugs against SARS-CoV-2 main protease (M pro) by using STD-NMR spectroscopy , in silico studies and antiviral assays. *International Journal of Biological Macromolecules* 234, 123540. <https://doi.org/10.1016/j.ijbiomac.2023.123540>

Nguyen, T.H., Mai, Q., Minh, T., Pham, Q., Thi, P., Minh, H., Thi, H., Phung, T., 2023. Machine learning combines atomistic simulations to predict SARS - CoV - 2 Mpro inhibitors from natural compounds. *Molecular Diversity* 1–9. <https://doi.org/10.1007/s11030-023-10601-1>

Podgorelec, V., Kokol, P., Stiglic, B., Rozman, I., 2002. Decision Trees : An Overview and Their Use in Medicine. *Journal of Medical Systems* 26, 445–463.

Rokach, L., 2016. Decision forest : Twenty years of research. *INFORMATION FUSION* 27, 111–125. <https://doi.org/10.1016/j.inffus.2015.06.005>

Shah, B., Modi, P., Sagar, S.R., 2020. In silico studies on therapeutic agents for COVID-19 : Drug repurposing approach. *Life Sciences* 252, 117652. <https://doi.org/10.1016/j.lfs.2020.117652>

Simeon, S., Anuwongcharoen, N., Shoombuatong, W., Malik, A.A., Prachayashittkul, V., Wikberg, J.E.S., Nantasesamat, C., 2016. Probing the origins of human acetylcholinesterase inhibition via QSAR modeling and molecular docking. *PeerJ* 4. <https://doi.org/10.7717/PEERJ.2322>

Su, Y., Wu, J., Li, X., Li, J., Zhao, X., Pan, B., Huang, J., Kong, Q., Han, J., 2023. DTSEA : A network-based drug target set enrichment analysis method for drug repurposing against COVID-19. *Computers in Biology and Medicine* 106969. <https://doi.org/10.1016/j.combiomed.2023.106969>

Suay-garcia, B., Falc, A., Bueso-bordils, J.I., Anton-fos, G.M., Teresa, M.P., Alem, P.A., 2020. Tree-Based QSAR Model for Drug Repurposing in the Discovery of New Antibacterial Compounds against Escherichia coli. *Pharmaceuticals* 13, 431.

Trott, O., Olson, A.J., 2010. Software News and Update AutoDock Vina : Improving the Speed and Accuracy of Docking with a New Scoring Function , Efficient Optimization , and Multithreading. *Journal of computational chemistry* 31, 455–61. <https://doi.org/10.1002/jcc>

Tsantili-kakoulidou, A., Demopoulos, V.J., 2021. Drug-like Properties and Fraction Lipophilicity Index as a combined metric. *ADMET & DMPK* 9, 177–190.

Wang, Y., Gao, Q., Yao, P., Yao, Q., Zhang, J., 2023. Multidimensional virtual screening approaches combined with drug repurposing to identify potential covalent inhibitors of SARS-CoV-2 3CL protease. *Journal of Biomolecular Structure and Dynamics* 1–24. <https://doi.org/10.1080/07391102.2023.2193994>

Yap, Wei, C., 2011. 16_J Comput Chem - 2010 - Yap - PaDEL-descriptor An open source software to calculate molecular descriptors and fingerprints.pdf. *Journal of computational chemistry* 32, 1466–74.